



Research Article

CeO₂-TiFe₂O₄ nanocomposite for effective removal of uranium ions from aqueous waste solutions

El Said A. Nouh¹ · T. A. Lasheen¹ · Rabab M. El-sherif² · N. A. Abdel Ghany³ · E. A. Jebri¹

© Springer Nature Switzerland AG 2019

Abstract

The present work deals with the preparation of Cerium oxide Titanium Ferrite (CTF) nanocomposite using a simple solvothermal method. The synthesized CTF nanocomposites were characterized using FT-IR, XRD, BET surface area, VSM and TEM. The adsorption action of CTF nanocomposite towards U(VI) was optimized using batch experiments by varying solution pH, initial concentration, sorbent dosage and rate of adsorption. The loaded uranium was efficiently desorbed using 0.1 M HNO₃. The Kinetic studies indicated that the adsorption process follows pseudo-second-order equation. Freundlich and Halsey adsorption isotherm was modeled, it proves the multilayers adsorption process. The calculated thermodynamic parameters show that the adsorption process of U(VI) onto CTF nanocomposite was spontaneous and endothermic in nature. The fabricated nanocomposite was applied successfully for removal of uranium species from waste solutions. The obtained results indicated that CTF nanocomposite was a promising and excellent adsorbent for uranium ions removal in comparison with other reported ones. Moreover, the process was very simple, fast and easily reusable several times.

Keywords Uranium · Magnetic · Nanocomposite · Adsorption · Waste solutions

1 Introduction

Uranium is a radioactive metal that is found in a variety of rocks, soils and aqueous sources. It is released into environment naturally or as contaminant through mining processing, fuel manufactures and other related industrial activities [1, 2]. In some contaminated regions waste disposal sites can attain as high as several tens of mg/L which eventually may found their way into soil, drinking water and human beings [3]. It leads to dangerous pollution and severe effect to human health [4–6], including, kidney tubular cells damage, liver disease and thyroid. Also, it affects bone development and maintenance, especially in children [7]. Due to uranium radioactivity may cause damage of DNA and can lead to several types of cancer [7, 8].

Over the past decades, several traditional methods have been developed to remove uranium ions from aqueous waste solutions such as membrane dialysis, precipitation, ion exchange, solid phase extraction and solvent extraction [9–14]. In this context, adsorption procedures have been found to offer much greater extraction capacity and efficiency.

Nanomaterials continue to attract much interest because of their properties differ greatly from those of atoms and molecules as well as from those of bulk Materials [15]. Using of nanoparticles (NPs) as adsorbents have been extensively studied because of their unique chemical and physical properties such as high surface area and chemical activity, compared to classical adsorbent materials [16]. Synthesis of nanometer scale

Electronic supplementary material The online version of this article (<https://doi.org/10.1007/s42452-019-0176-2>) contains supplementary material, which is available to authorized users.

✉ El Said A. Nouh, saidnouh81@yahoo.com | ¹Nuclear Materials Authority, P.O. Box 530 El Maadi, Cairo, Egypt. ²Department of Chemistry, Faculty of Science, Cairo University, Cairo, Egypt. ³Physical Chemistry Department, National Research Centre, Cairo, Egypt.

SN Applied Sciences (2019) 1:159 | <https://doi.org/10.1007/s42452-019-0176-2>

Received: 4 October 2018 / Accepted: 9 January 2019

Published online: 14 January 2019

SN Applied Sciences
A SPRINGER NATURE journal

mixed oxide particles, such as spinel ferrite, magnetite, titanium-based various binary and ternary mixed oxides have been reported for their remarkable magnetic and conducting properties [17–20]. The use of iron oxide NPs has found many applications in a variety of fields. Both forms of magnetic iron oxide NPs, Fe_2O_3 and Fe_3O_4 , have superparamagnetic properties, enabling them to behave as a giant paramagnetic atom with a fast response to the external magnetic field. Magnetic NPs are suitable sorbents due to their good dispersion in solution, their high specific surface area and their ability to be controlled and separated with an external magnetic field [16, 17]. Also, TiO_2 exhibits very favorable sorption properties through inner-sphere complex formation [21, 22]. The incorporation of titanium and cerium ions with ferrites NPs leads to an increase of coercivity due to the coupling of the spins between titanium and cerium ions on hand and iron ions on other [23, 24]. This behavior makes the NPs to be more efficient and attractive in separation of impurities from different effluents.

Lichao Tan et al. [25] suggested cobalt ferrite/multi-walled carbon nanotubes magnetic hybrids for removal of U(VI) from wastewater. They pointed out that the maximum capacity for U(VI) was 212.7 mg/g under optimum conditions. Magnetic nanocomposite ($\text{Fe}_3\text{O}_4@\text{C}@\text{Ni}-\text{Al}$ LDH) of U(VI) adsorption capacity of 174.1 mg g^{-1} was reported by Zhang et al. [26]. Fan et al. [27] investigated removal of U(VI) from aqueous solutions by magnetic composite of $\text{Fe}_3\text{O}_4@\text{SiO}_2$, showing maximum adsorption capacity of uranyl ions of 52 mg g^{-1} . Other reported modified magnetic nanoparticles showed moderate sorption capacities for uranyl ions and radioactive species [28–31].

In our previous work we reported the synthesis of $\text{TiO}_2-\text{CeO}_2-\text{Fe}_2\text{O}_3$ nanoparticles (NPs) using co-precipitation method for using in U(VI) removal from aqueous solutions [32]. Herein, we extended our study for preparation of an efficient magnetic nanocomposite ($\text{CeO}_2-\text{TiFe}_2\text{O}_4$) using simple and fast solvothermal method in order to use for removal of uranium ions from waste samples solutions. The prepared CTF nanocomposites were characterized by X-ray diffraction (XRD), scanning electron microscope (SEM), transmission electron microscope (TEM), Brunauer-Emmett-Teller surface area (BET), Fourier Transform Infra-Red spectroscopy (FTIR) and vibrating sample magnetometer (VSM). The optimum parameters that influence the adsorption of U(VI) by CTF NPs, including pH, contact time, adsorbent dosage, U(VI) initial concentration and temperature were discussed. Isotherm models were proposed to explain the sorption characteristics of nanoadsorbents. Kinetic and thermodynamic parameters of the adsorption process were also calculated to discuss the adsorption process.

2 Experimental

2.1 Materials

All chemicals and reagents were of an analytical grade. TiCl_4 ($\geq 99\%$, Merck Co.Ltd., France), $\text{CeCl}_3 \cdot 7\text{H}_2\text{O}$ (Sigma Chemical Co. Ltd., USA), $\text{FeSO}_4 \cdot 7\text{H}_2\text{O}$ ($> 98\%$, Nice Chemicals Pvt. Ltd. India) ethanol (absolute, (Sigma Aldrich Co. Ltd., USA) were used without further purification. Uranium (IV) stock solution (1000 mg L^{-1}) was prepared by dissolving 2.11 g of $\text{UO}_2(\text{NO}_3)_2 \cdot 6\text{H}_2\text{O}$ (Sigma-Aldrich, Germany) in 1 L of 0.05 M HNO_3 .

2.2 Synthesis of $\text{CeO}_2-\text{TiFe}_2\text{O}_4$ nanoadsorbent

$\text{CeO}_2-\text{TiFe}_2\text{O}_4$ NPs were prepared by using solvothermal method. Stoichiometric amounts of 2 M $\text{FeSO}_4 \cdot 7\text{H}_2\text{O}$, 0.5 M TiCl_4 and $\text{CeCl}_3 \cdot 7\text{H}_2\text{O}$ were dissolved in a mixture of 60 mL of ethylene glycol and 40 mL of de-ionized water while stirring for 30 min then sonicated using an ultrasonic processor for 15 min. To the latter, ammonia solution was added drop wisely, sonicated for 15 min, then heated to 180 °C for 24 h in a Teflon-lined autoclave. After cooling down to room temperature, the precipitate was centrifuged, collected and washed repeatedly with de-ionized water and ethanol then dried for 12 h at 60 °C.

2.3 Characterization

XRD characterization of the prepared nanocomposite was carried out using (X, PERT—PRO—PANalytical—Netherlands) with $\text{CuK}\alpha$ radiation operating at 40 kV and 30 mA. FT-IR measurements were made with JASCO FTIR 460 plus spectrometer over wavenumber range of 4000–400 cm^{-1} . The spectra of magnetic nanomaterials were taken as KBr pellets.

The size and morphology of the nanocomposites before and after sorption were examined by high resolution transmission electron microscopy (A JEOL-2100) and scanning electron microscopy equipped with EDX (ESEM model Philips XL 30).

The surface area and pore volume of magnetic nanoadsorbents were measured by performing N_2 adsorption and desorption using surface area and porosity analyzer (AUTOSORB-1, Model No = AS1 MPV6-11, USA) and the surface area was calculated by Brunauer–Emmett–Teller (BET) equation as well. However, pore size distributions were calculated from the adsorption branch of the N_2 adsorption/desorption isotherms using the Barret–Joyner–Halenda (BJH) method. Magnetic characteristics of the prepared

nanocomposites were measured by vibrating sample magnetometer (VSM).

2.4 Batch adsorption experiments

To achieve adsorption equilibrium, an amount of the adsorbent (0.005 g) was added into U(VI) solution in polyethylene tube. The pH was adjusted to the desired value by 0.1 M HNO₃ and NaOH solutions. The mixture was shaken for 2 h in a temperature controlled water bath shaker. After equilibrium, the supernatant liquids were centrifuged. The residual U(VI) concentration in supernatant was spectrophotometrically determined using arsenazo-III at wavelength 655 nm [33]. The effects of pH, contact time, initial concentrations and temperature on adsorption of uranium (VI) were investigated to obtain the maximum efficiency.

The removal efficiency (%) and the adsorption capacity (mg g⁻¹) of U(VI) were determined using.

Equations (1) and (2), respectively:

$$R = \frac{C_0 - C_e}{C_0} \times 100\% \quad (1)$$

$$q_e = \frac{(C_0 - C_e)V}{W} \quad (2)$$

where R is the removal efficiency, C₀, C_e is the initial and equilibrium U(VI) concentration (mg L⁻¹), respectively, q_e is adsorption capacity, V is the volume of uranium solution (L) and W is the weight of CTF nanoadsorbent (g).

2.5 Desorption and regeneration

Firstly, Uranium(VI) loaded CTF nanocomposite was washed several times with de-ionized water then 0.1 mol L⁻¹ HNO₃ was used as eluting agent to desorb U(VI). The adsorbents were separated from the solution by centrifugation, then the CTF nanocomposites were dried and reused in adsorption experiments. The above procedure was repeated six times to test the reusability of the magnetic nanoadsorbents until U(VI) were not detected in the rinsing solution. The desorption efficiencies were calculated from the concentration of adsorbed U(VI) onto CTF nanoadsorbent and the final U(VI) concentration in the desorption medium.

3 Results and discussions

3.1 Characterization of nanoadsorbent

A typical X-ray diffraction pattern of the prepared CTF nanocomposite is shown in Fig. 1. As can be seen, the major characteristic peaks of TiFe₂O₄ were found at

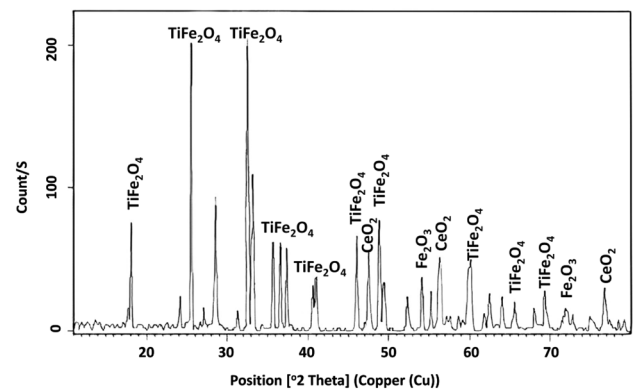


Fig. 1 XRD patterns of synthesized CTF nanocomposite

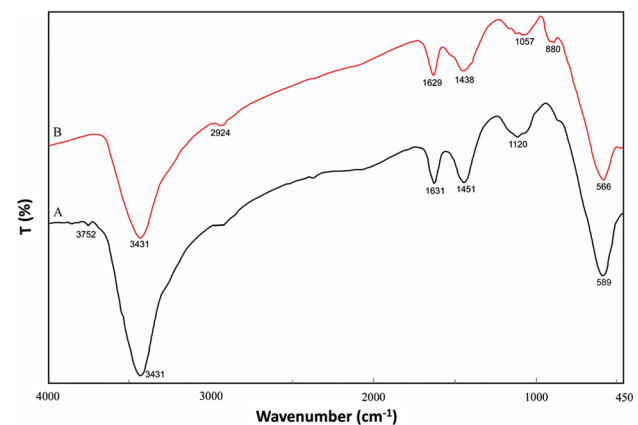


Fig. 2 FT-IR of CTF nanoparticles (A) before U(VI) adsorption (black line) and (B) after U(VI) adsorption (red line)

$2\theta = 18.102, 25.535, 32.522, 36.550, 37.345, 41.03, 45.9, 48.791, 59.8, 65.5, 69.3$ and 76.7 , references code (04-008-6392). On the other hand the cubic CeO₂ peaks were identified at $2\theta = 28.550, 33.077, 47.490$ and 56.328 corresponding to references code (00-04-0593). Additional peaks observed at $2\theta = 54.02$ and 72.2 are due to Fe₂O₃. According to the above mentioned XRD results, we can conclude that the structure of the nanocomposite is CeO₂-TiFe₂O₄.

FT-IR spectrum of CTF nanocomposite before and after loading by uranium species were presented in Fig. 2. The two broad bands observed at 3431 cm^{-1} and 1631 cm^{-1} were due to the O-H stretching vibrations, however, the small peaks observed at 2924 and 1451 cm^{-1} were due to C-H stretching vibration and C-H bending, respectively, they were attributed to presence of ethylene glycol on the surface of CTF nanocomposite [34, 35]. The band at 1120 cm^{-1} was due to presence of CeO₂ [36]. While the absorption band located at 589 cm^{-1} was assigned to the stretching vibration band of Fe-O bond. As a consequence

of uranium adsorption onto nanocomposite surface, a new band was appeared at 880 cm^{-1} which may be attributed to antisymmetric stretching vibration of $\text{O}=\text{U}=\text{O}$ bands, confirming a successful U(VI) sorption as uranyl ions or uranyl complexes [37]. The lack of the strong peak at 1380 and 1530 cm^{-1} for CTF nanoadsorbent after loading with U(VI) clearly indicates that no nitrate ions as counter ions or chelating agent was co-sorbed with U(VI) [38]. In such case, the U(VI) ions were probably sorbed in hydroxide complex form or positive charge species by cation-exchange mode [38]. Also, the nanocomposite characteristic bands were slightly shifted and become less intense after uranium adsorption onto CTF nanocomposite, Fig. 2b. After adsorption process, the formed uranium layers on the surface of the nanoadsorbent reduces the intensities of the characteristic bands of CTF nanocomposite as well as causing a shift of their positions. The bands of Fe-O , CeO_2 , C-H and O-H were shifted from 589 , 1120 , 1451 , 1631 cm^{-1} to be 566 , 1057 , 1438 and 1629 cm^{-1} , respectively, after uranium loading on to CTF nanoadsorbent. The shift of bands due to adsorption of uranium was also reported by others [14, 39].

The size, distribution and morphology of the prepared nanoparticles (NPs) were examined by, TEM, HRTEM and

EDX techniques as shown in Fig. 3. The TEM images show that CTF NPs are polydispersed with particle size ranged from 1.91 to 19 nm . The measured inter-planar spacing and the lattice d-spacing of $\text{CeO}_2\text{-TiFe}_2\text{O}_4$ were 0.12 nm and 1.1 nm , respectively. The agglomeration of the nanoparticles can be well observed, pertaining to the high surface energy and magnetic interactions between them [40].

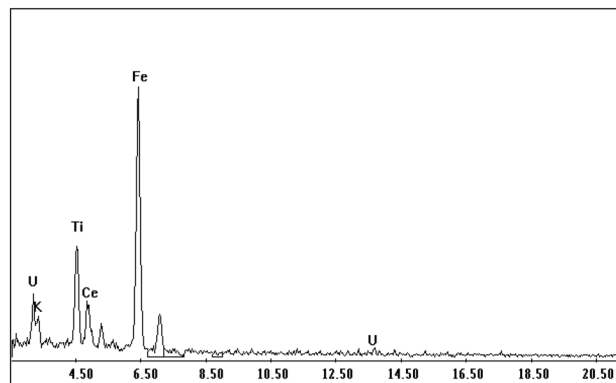


Fig. 4 EDX spectrum analysis of $\text{CeO}_2\text{-TiFe}_2\text{O}_4$ nanocomposite loaded by U(VI)

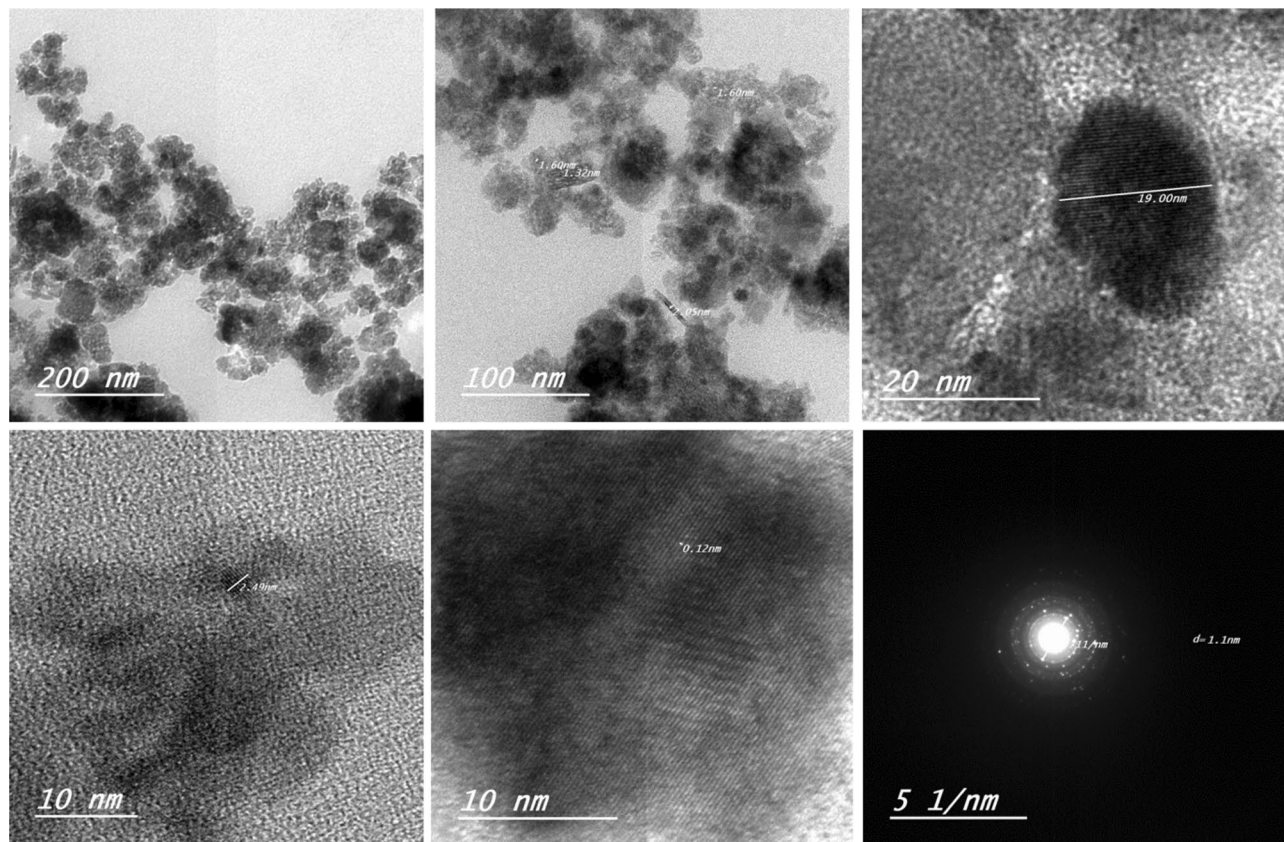
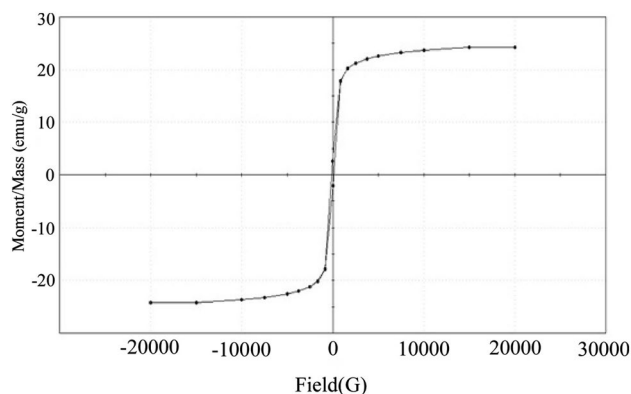


Fig. 3 TEM images of CTF nanoparticles

Table 1 Physical parameters of CTF nanoadsorbent

| Particles size (nm) | Surface area (m ² /g) | Pore volume (CC/g) | Pore radius (nm) | Magnetization (emu/g) | Remenace (emu/g) | Coercivity (H _{ci}) (G) |
|---------------------|----------------------------------|--------------------|------------------|-----------------------|------------------|-----------------------------------|
| 1.9-19 | 72.459 | 0.118 | 1.925 | 24.193 | 2.3677 | 97.96 |

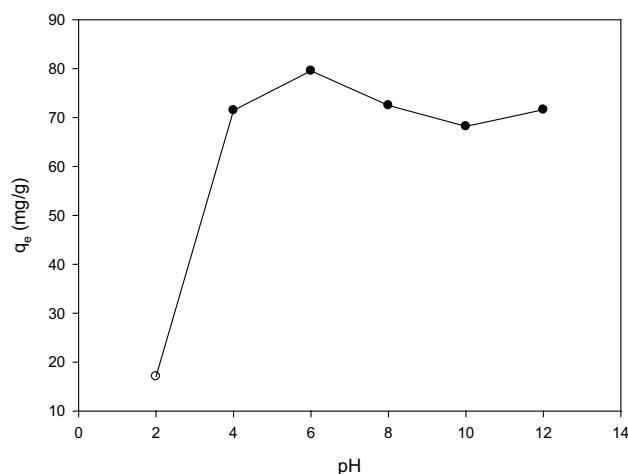
**Fig. 5** VSM hysteresis loops of CeO₂-TiFe₂O₄ nano hybrid oxide

The presence of uranium in the loaded CeO₂-TiFe₂O₄ nanoadsorbent was confirmed from (EDX) measurement, Fig. 4. It shows distinct signals at 3.3 and 3.4 keV corresponding to uranium species, it was sufficient for providing a qualitative idea of the homogeneous distribution of U ions at the surface of the sorbent, the percentage (in mass) of U was 30.72 and 26.78%, respectively.

BET surface area measurements are performed and summarized in Table 1. The surface area, pore volume, and pore size of CeO₂-TiFe₂O₄ are 72.459 m²/g, 0.118 cc/g, and 1.925 nm, respectively. Also, BET results confirmed the formation of nano-scale size CeO₂-TiFe₂O₄ particles. The obtained parameters assured the good adsorption behavior of the CTF nanocomposite.

3.2 Magnetic properties

Chemical composition of magnetic materials, cation distribution and average size have a significant role in the determination of the magnetic properties of the NPs and the possible applications [41]. The magnetic properties of CTF NPs are investigated at the ambient temperature under an applied field using the VSM technique. Figure 5 shows the hysteresis loops of the CTF nanocomposite. It exhibited superparamagnetic behavior with a high magnetic saturation M_s value of 24.193 emu/g at room temperature. The magnetic properties of CTF NPs were found good in comparison with that of TiO₂-CeO₂-Fe₂O₃ NPs previously reported by us [32], where the saturation magnetization of the latter was 0.32096 emu/g. The hysteresis

**Fig. 6** Effect of initial pH on adsorption capacity of CeO₂-TiFe₂O₄ (amount of adsorbent 0.005 g, U(VI)_{initial} = 20 mg L⁻¹, shaking time 120 min at 25 °C)

loop of TiO₂-CeO₂-Fe₂O₃ showed paramagnetic behavior. In addition, it was observed that the magnetization of TiO₂-CeO₂-Fe₂O₃ is not saturated, as it is probably due to the coexistence of paramagnetic atoms in the particles. On the other side CeO₂-TiFe₂O₄ nanoparticles exhibited good magnetic properties (M_s 24.193 emu/g). The hysteresis loop of CeO₂-TiFe₂O₄ confirmed its ferromagnetic behavior as the magnetization reached saturation. Furthermore, the calculated normalized remanence values (M_r) and the coercivity (H_c) were 2.367 and 97.961 G, respectively. These results indicate that CeO₂-TiFe₂O₄ NPs possesses a high magnetic responsiveness and can be easily separated during the sorption experiments.

3.3 Adsorption process

3.3.1 Effect of initial pH

A series of experiments were performed to investigate the effect of solution pH on uranium uptake by CTF NPs. The obtained results in Fig. 6 showed that the adsorption capacity of uranium increased from 17.08 to 79 mg g⁻¹ as the pH increased from 2.00 to 6.00. By increasing the pH more than 6.00, the adsorption capacity was slightly decreased to reach 71.6 mg g⁻¹ at pH 12.00. The lower adsorption capacity at low acidic conditions is due to

competition of H^+ for binding sites of CTF nanocomposite with UO_2^{2+} ions. However, the adsorption capacity reaches maximum at pH 6. At such pH the NPs surface became negatively charged due to deprotonation reaction [42] and the electrostatic attraction increased between uranium species and negative charge on nanoparticles surface which led to an increase of U(VI) adsorption capacity. The distribution of uranium chemical species is represented in scheme S1 [43]. It is obvious that uranyl ions may present as positively charged cationic species, such as UO_2^{2+} monomer, $[(UO_2)_2(OH)_2]^{2+}$ dimer and $[(UO_2)_3(OH)_5]^+$ trimer [44, 45]. Multi-nuclear hydroxide complexes such as $[(UO_2)_3(OH)_5]^+$ are the predominate species at pH 6 and no insoluble species were observed. These species may be more favored by the sorbent, since the maximum sorption of U(VI) in many different sorbents occurred at pH 6–8 [46, 47]. The deprotonated sites of CTF nanoadsorbent are more available to retain uranium ions and surface complexation between uranium species and CTF nanoparticles is facilitated. At $pH > 6.00$ uranium ions exist in an anionic forms such as $UO_2(CO_3)_3^{4-}$, $(UO_2)_2CO_3(OH)_3^-$, $UO_2(OH)_3^-$ etc. [48], these anions have a relatively low adsorption affinity. Thus, pH 6.00 was chosen as optimum for adsorption process.

3.3.2 Effect of CTF composite dose

The dependence of U(VI) removal on amount of adsorbent was studied at pH 6 using 20 mL of 20 mg L^{-1} U(VI) solution at 25 °C for 120 min. The results given in Fig. 7, demonstrate that the sorption efficiency of uranium ions increases rapidly with increasing sorbent mass from 1 mg to 5 mg. This is due to large number of active centers on the surface [49].

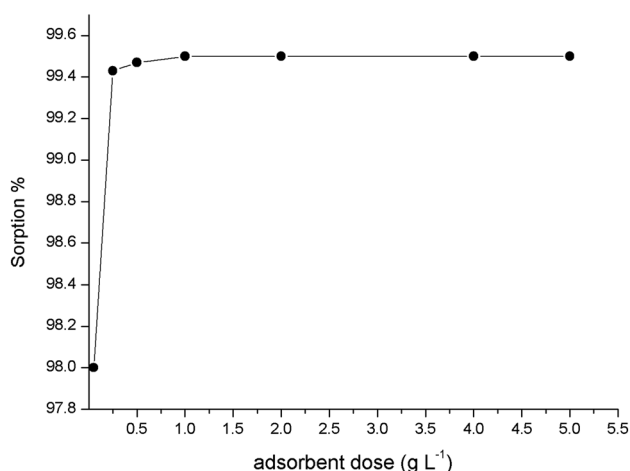


Fig. 7 Effect of adsorbent amount on U(VI) uptake by CTF nanoparticles (pH 6.00; amount of adsorbent dose 0.001–0.1 g; $[U(VI)]_{initial}$ 20 mg L^{-1} ; shaking time 120 min)

3.3.3 Effect of contact time and adsorption dynamics

The contact time effect on U(VI) uptake capacity of CTF nanocomposite was studied using different U(VI) initial concentration (20, 50 and 70 mg L^{-1}). The obtained results in Fig. 8, showed that the maximum amount of U(VI) was adsorbed at 120 min for the three tested concentrations. The maximum adsorption capacity (q_e) was 79, 178 and 245 mg g^{-1} , corresponding to U(VI) initial concentration of 20, 50 and 70 mg L^{-1} , respectively. There is almost no further increase of adsorption beyond 120 min and the initial concentration did not show any significant effect on the time to reach equilibrium. It proves that the U(VI) adsorption capacity increases with its initial concentration increasing. It provides higher driving force that facilitates diffusion of ions from the bulk solution to active sites assembly. Thus the initial U(VI) concentration plays an important role in determining the maximum uptake capacity of the CTF for U(VI) [50].

Adsorption kinetics is one of the most attractive characteristics to be responsible for the efficiency of adsorption. It is useful for adsorption studies to predict the rate of adsorption and provide valuable data for understanding the mechanism of sorption and the reaction pathways. Actually, most adsorption reactions take place through external film diffusion, intra-particle diffusion and interaction between adsorbate and active sites. Sorption of uranium by the CTF NPs as a function of time was illustrated in Fig. 8. It showed clearly a fast increase in uptake of uranium ions by CTF NPs in the first 2 h of the adsorption then remains constant. The obtained data were modeled using pseudo-first-order, pseudo-second-order and intra-particle diffusion.

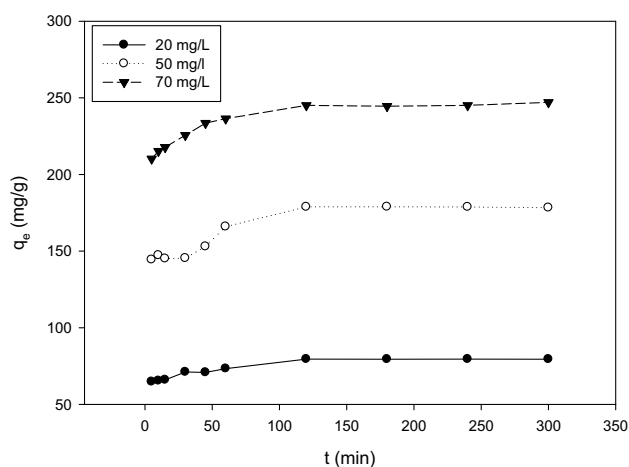


Fig. 8 Effect of contact time on uranium(VI) adsorption using different initial uranium concentration (pH 6.0; temperature 25 °C; amount of CTF NPs 0.005 g)

The pseudo-first-order was calculated according to equation (S1) in Supporting Information (SI). The obtained results of pseudo-first-order adsorption featured in Fig. 9a, indicate that the data did not fit well. The values of K_1 along with the corresponding correlation coefficient at different concentrations are presented in Table 2. As shown, the calculated values of q_e does not agree with the experimental ones besides its low related coefficients R^2 . These results indicate that the adsorption mechanism of uranium

ions on CTF does not follow a pseudo-first-order kinetic model well.

In order to study pseudo-second-order adsorption (see equation S2) a plot of t/q_t versus t is plotted in Fig. 9b. The obtained straight line and the perfect regression analysis $R^2 = 0.999$ prove that the pseudo-second-order kinetic model can be applied to predict the adsorption kinetic, and the process of uranium sorption on CTF NPs is well described by pseudo second order kinetic model, Table 2. It implies that the dominant mechanism for U(VI)

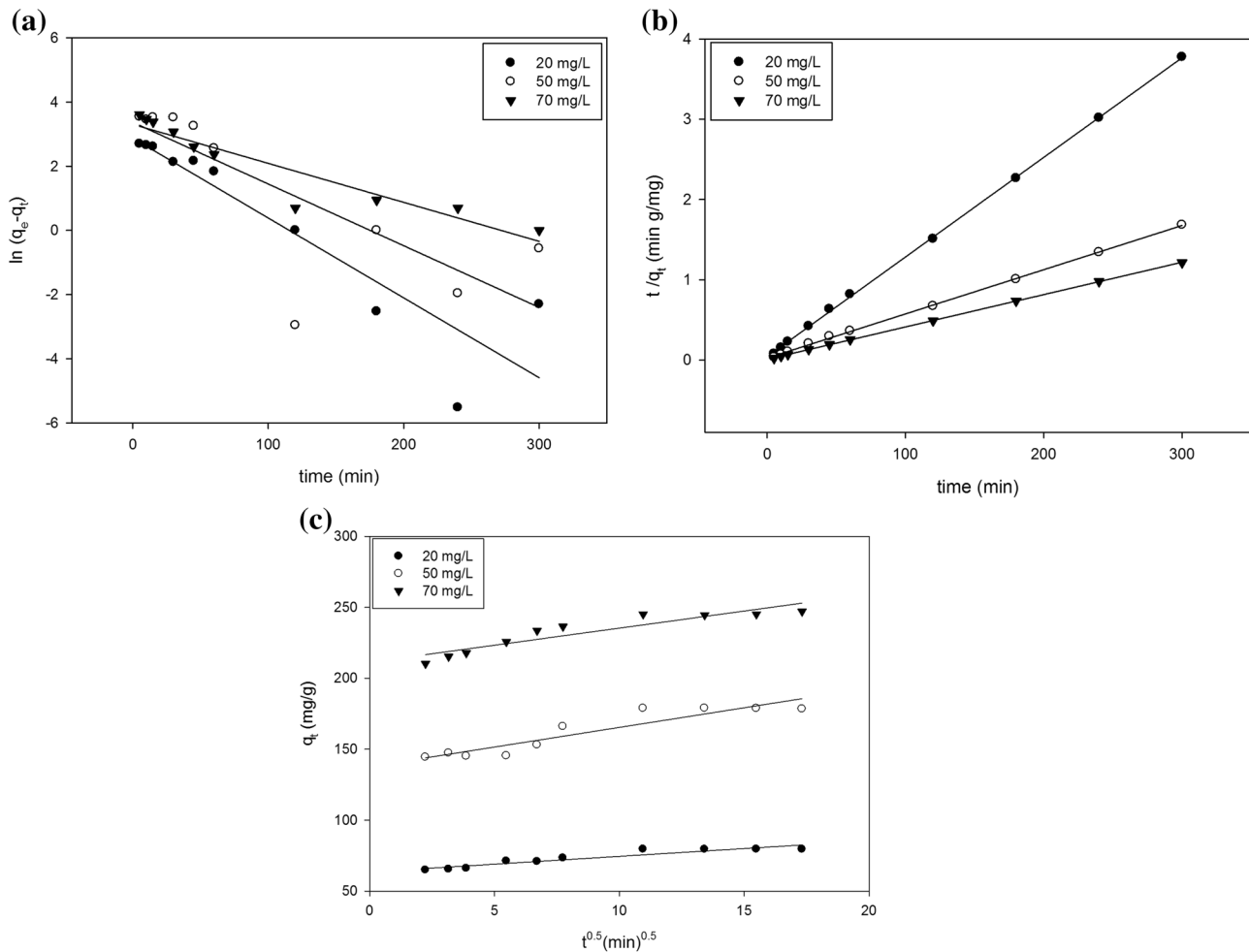


Fig. 9 Adsorption kinetics models for U(VI) adsorption onto CTF nanocomposite, **a** Pseudo-first-order model plot. **b** Pseudo-second-order model plot. **c** Intra-particle diffusion model plot. Conditions (pH 6.0; temperature 25 °C; amount of CTF NPs 0.005 g)

Table 2 Parameters of various kinetics models fitted to experimental data

| C_0 (mg L ⁻¹) | Pseudo first order | | | Pseudo second order | | | Intraparticle diffusion | | |
|-----------------------------|-----------------------------|----------------------------|-------|-----------------------------|---|--------|---------------------------|-------|-------|
| | q_e (mg g ⁻¹) | K_1 (min ⁻¹) | R^2 | q_e (mg g ⁻¹) | K_2 (g mg ⁻¹ min ⁻¹) | R^2 | C (mg g ⁻¹) | K_i | R^2 |
| 20 | 17.67 | 0.0249 | 0.834 | 80.65 | 0.00365 | 0.9997 | 63.471 | 1.098 | 0.888 |
| 50 | 28.99 | 0.0192 | 0.632 | 181.82 | 0.00123 | 0.9995 | 137.60 | 2.767 | 0.862 |
| 70 | 28.41 | 0.0123 | 0.889 | 250 | 0.00184 | 0.9999 | 210.71 | 2.421 | 0.879 |

adsorption on CTF NPs is chemisorption or strong surface complexation rather than mass transport [51].

To identify the mechanism involved in the adsorption by the intra-particle diffusion technique (see equation S3) a plot of $t^{1/2}$ versus q_t was represented in Fig. 9c. The values of K_i (the intra-particle diffusion rate constant $\text{mg g}^{-1} \text{min}^{-1/2}$) and C adsorption constant (thickness of the boundary layer) are calculated from intercept and slope regression analysis [52–56]. The results in Table 2 show that the experimental data does not follow the intra-particle diffusion model, i.e. the intra-particle diffusion is not rate limiting step.

3.3.4 Adsorption isotherm

In this study, several isotherm models were selected to fit the obtained experimental data regarding to the adsorption of uranium onto CTF NPs. They are namely Langmuir, Freundlich, Temkin, Dubinin Radushkevich (D–R) and Halsey models.

Langmuir isotherm model was described by equation S4. The plot of C_e/q_e versus C_e at different temperatures was shown in Fig. 10a. The values of Q_m and K_L can be estimated from the slopes and intercepts of the straight lines, Table 3. Adsorption of U/CTF NPs exhibited maximum sorption capacity of 476.2 mg of U(VI)/g of sorbent at pH 6 from aqueous solutions. The sorption capacity of CTF nanoparticles was found greater than that obtained by $\text{TiO}_2\text{-CeO}_2\text{-Fe}_2\text{O}_3$ nanoparticles previously reported by us [32]. Table 4 showed comparison of CTF nanoparticles sorption capacity with other reported ones. It indicated that CTF nanoparticles are an excellent adsorbent for uranium ions.

The essential features of the Langmuir isotherm model expressed in terms of a dimensionless constant separation factor or equilibrium parameter R_L [57], which is defined by equation S5. In this study, the values of R_L lie between 0.041 and 0.446 for all concentration and temperature ranges. This indicates the suitability of the CTF as an adsorbent for adsorption of uranium ions from aqueous solution under the conditions used in this study.

The Freundlich model is expressed by equation S6. The linear plot of $\ln q_e$ versus $\ln C_e$ is presented in Fig. 10B.

It was reported that the Freundlich isotherm constant can be used to explore the favorability of adsorption process. When value of n within $1 < n < 10$, it gives an indication of the favorability of adsorption. In our work it was found that the values of n are situated in this range Table 3, implies stronger interaction between sorbent and uranium ions demonstrating that the adsorption process is favorable.

The Halsey adsorption isotherm was given by equation S7 and the isotherm parameters were obtained from the plot of $\ln q_e$ versus $\ln (1/C_e)$, Table 3. Definitely, the fitting of the experimental data to this equation attest to the heteroporous nature of the adsorbent, Fig. 10c.

The Temkin isotherm was expressed by equation S8. The calculated isotherm parameters are listed in Table 3 and illustrated in Fig. 10d. The linear plot of q_e versus $\ln C_e$, Fig. 10d, yields the constant b_T from 0.023 to 0.029 suggesting chemisorption and physisorption involved in the adsorption of the U(VI) ions. On the other hand, the greater values of A_T indicate greater affinity toward the adsorbate [58].

The simple linear form of D–R isotherm is represented in equation S9. The plot between $\ln q_e$ and ϵ^2 (Fig. 10e) yields the constant K which is used to calculate the mean free energy E of sorption per molecule of the sorbate when it is transferred to the surface of the solid from infinity in the solution (see equations S10 and S11) [59].

The estimated values of E lie between 7.2 and 7.6 kJ mol^{-1} indicating the physisorption mechanisms. Based on the data given in Table 3, the Freundlich and Halsey models appear to be the best fitting models for uranium adsorption depending on correlation coefficient R^2 where it is very high than Langmuir, Temkin and D–R models.

3.3.5 Effect of temperature and adsorption thermodynamics

The adsorption experiments at different temperatures were performed to evaluate the influence of temperature (25–55 °C), Fig. 11. The results showed that the adsorption of uranium ions is favored by an increase in temperature. The temperature dependence of the adsorption process is associated with changes in several thermodynamic parameters such as enthalpy (ΔH) and entropy (ΔS) of adsorption, which are calculated from the slope and intercept of the linear variation of $\ln K_d$ versus $1/T$, Fig. 12, using the following equation:

$$\ln K_d = -\frac{\Delta H^\circ}{RT} + \frac{\Delta S^\circ}{R} \quad (3)$$

where K_d is the distribution coefficient (mL/g), T is absolute temperature (K), and R is the ideal gas constant ($8.314 \text{ kJ mol}^{-1} \text{ K}^{-1}$). The standard free energy values (ΔG) are calculated from:

$$\Delta G^\circ = \Delta H^\circ - T\Delta S^\circ \quad (4)$$

The obtained thermodynamic parameters from Eqs. (3) and (4) are presented in Table 5. The positive value of ΔH° confirms the endothermic nature of adsorption.

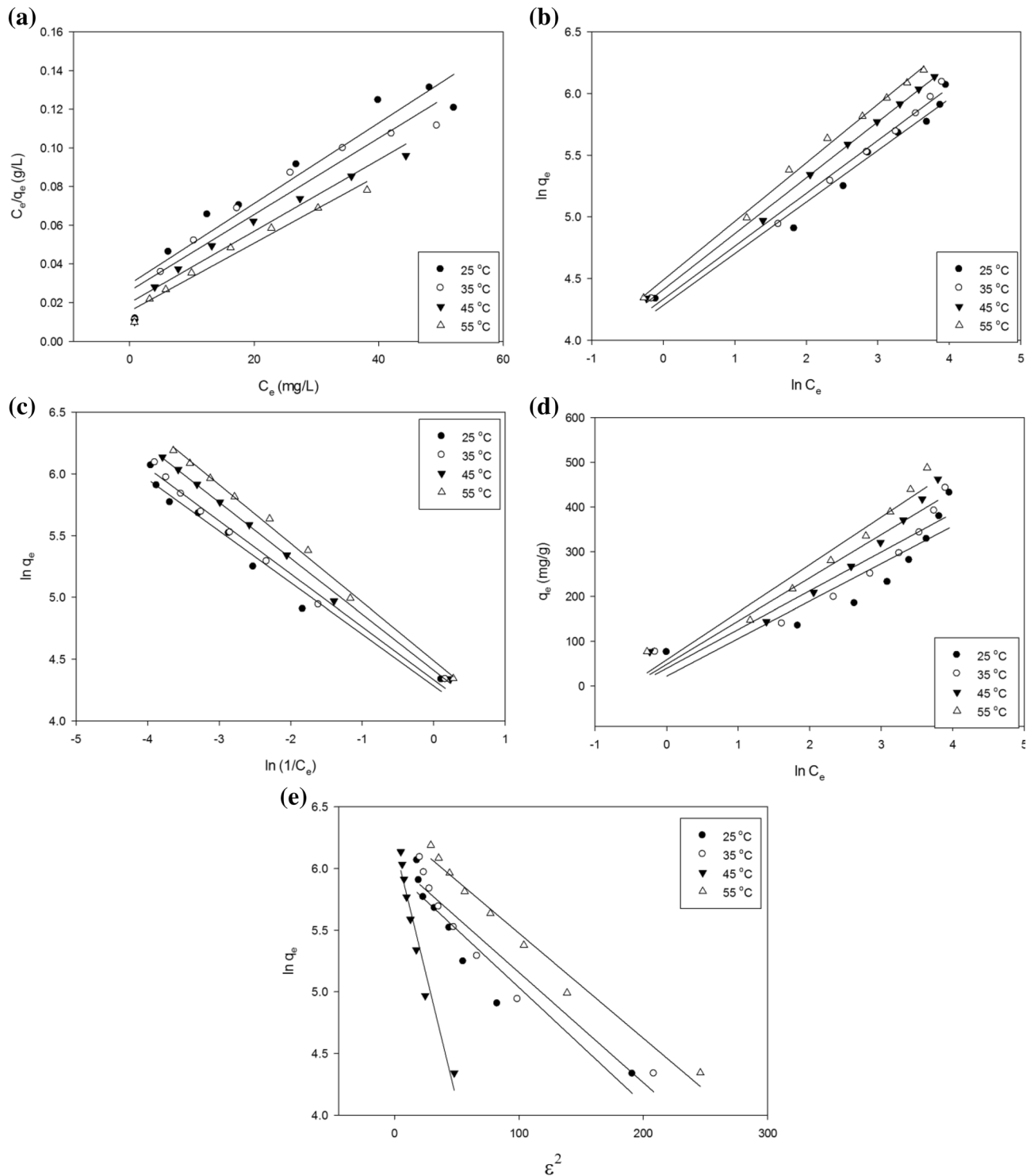


Fig. 10 Adsorption isotherms for U(VI) adsorption onto CTF nanocomposite, **a** Langmuir isotherm plot, **b** Freundlich isotherm plot, **c** Halsey isotherm plot, **d** Temkin isotherm plot, **e** D-R isotherm plot. Conditions (pH 6.00; temperature 25–55 °C; amount of CTF NPs 0.005 g)

Table 3 Parameters of various isothermal models fitted to experimental data

| Isotherm models | Parameters | 25 °C | 35 °C | 45 °C | 55 °C |
|---------------------|------------|--------------------|--------------------|--------------------|--------------------|
| Langmuir | Q_m | 476.2 | 500.0 | 555.5 | 555.5 |
| | K_L | 0.071 | 0.076 | 0.090 | 0.115 |
| | R^2 | 0.919 | 0.927 | 0.961 | 0.974 |
| Freundlich | K | 72.48 | 76.17 | 82.27 | 88.27 |
| | n | 2.391 | 2.336 | 2.207 | 2.107 |
| | R^2 | 0.974 | 0.989 | 0.997 | 0.996 |
| Halsey | K | 3×10^{-5} | 4×10^{-5} | 5×10^{-5} | 7×10^{-5} |
| | n | 2.391 | 2.332 | 2.207 | 2.107 |
| | R^2 | 0.974 | 0.989 | 0.997 | 0.996 |
| Temkin | b_T | 0.029 | 0.028 | 0.025 | 0.023 |
| | A_T | 1.303 | 1.583 | 1.656 | 0.554 |
| | R^2 | 0.824 | 0.882 | 0.923 | 0.949 |
| Dubini–Radushkevich | q_{max} | 394.5 | 424.9 | 489.4 | 560.4 |
| | E | 7.293 | 7.495 | 3.471 | 7.600 |
| | R^2 | 0.897 | 0.924 | 0.955 | 0.978 |

The positive value of ΔS° shows the increase of randomness at the solid–liquid interface during the adsorption of U(VI) onto CTF NPs. The positive entropy (ΔS°) favors complexation and stability of sorption [60]. Positive change in entropy favors a slower sorption of U(VI) onto active sites of the adsorbent. This result is in agreement with the fact that uranium sorption attains an equilibrium within 120 min. Also, it is compatible with the results of the kinetic studies. Where the adsorption process was described by pseudo second order kinetic model which implies that the dominate mechanism is surface complexation or chemisorption.

According to Table 5, all values of ΔG° are negative, which indicate the feasibility of the adsorption process

and the spontaneous nature of adsorption. With an increase of temperature, the values of ΔG° are more negative, which suggests that the equilibrium capacity increases. From the above results, the performance of U(VI) sorption on the as-prepared adsorbent is more favorable at higher temperatures.

3.3.6 Desorption and regeneration

Regeneration of CTF NPs was investigated to evaluate its potential application in the removal and recovery of uranium species. The data illustrated in Fig. 13, implies that the adsorbed ions can be desorbed from spent adsorbent in an acid medium. Hence, desorption study was conducted using HNO₃ solution having concentration range between 0.01 and 1 M. The desorption efficiency of HNO₃ concentrations of 0.01, 0.05, 0.1, 0.5 and 1 M was found 92.18%, 93.54%, 98.96%, 98.92%, 98.64%, respectively. Therefore, 0.1 M HNO₃ was determined as optimum desorptive concentration. To assess the reusability of the adsorbent, the adsorption–desorption experiments with 0.1 M HNO₃ was repeated six cycles. The adsorption efficiency of the CTF NPs decreased from 98.96% in the first cycle to 89.8% in the six cycles (Fig. 14). These entire make the CTF NPs to be used as a good and efficient adsorbent in waste management of radioactive species.

3.3.7 Application

The fabricated nanocomposite was used for removal of U(VI) from waste solutions derived from routine operations of uranium concentrate purification at Nuclear Material Authority (NMA), Anshas, Egypt. Figure 14 indicated the successful removing of uranium species from derived wastes of different concentration.

Table 4 Comparison of CTF nanoadsorbent capacity towards U(VI) with the other reported ones

| Adsorbent material | Initial pH | Contact time (min) | Temperature (°C) | Adsorption capacity(mg/g) | References |
|---|------------|--------------------|------------------|---------------------------|------------|
| CoFe ₂ O ₄ /MWCNTs | 6 | – | – | 212.7 | [25] |
| Fe ₃ O ₄ /GO | 5.5 | – | 20 | 69.5 | [61] |
| Fe ₃ O ₄ @SiO ₂ | 5 | – | 25 | 105.5 | [62] |
| Magnetite | 5 | – | 27 | 27 | [18] |
| Iron oxyhydroxide | 6 | – | – | 278 | [31] |
| MnO ₂ -Fe ₃ O ₄ -rGO | 6 | – | 55 | 108.7 | [19] |
| Cerium vanadate | 1–6 | – | – | 18.73 | [63] |
| Si-6G PAMAM | 4.5 | – | 25 | 303 | [14] |
| CoFe ₂ O ₄ | 6 | 180 | 25 | 170.07 | [20] |
| CTF NPs | 6 | 120 | 25 | 476.2 | This work |

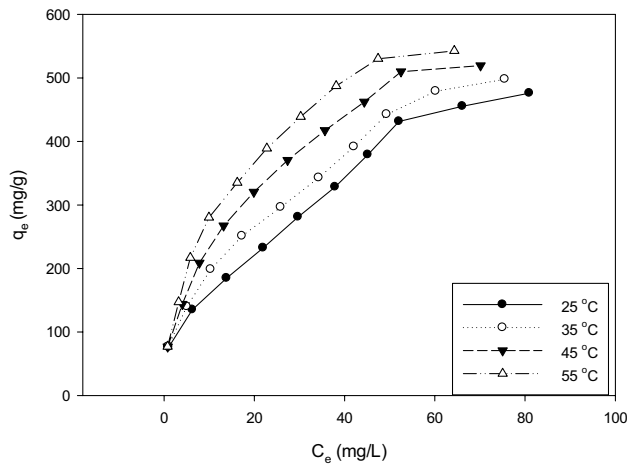


Fig. 11 Adsorption isotherm of U(VI)/CTF NPs at different temperatures (pH 6.0; temperature 25–55 °C; amount of CTF NPs 0.005 g)

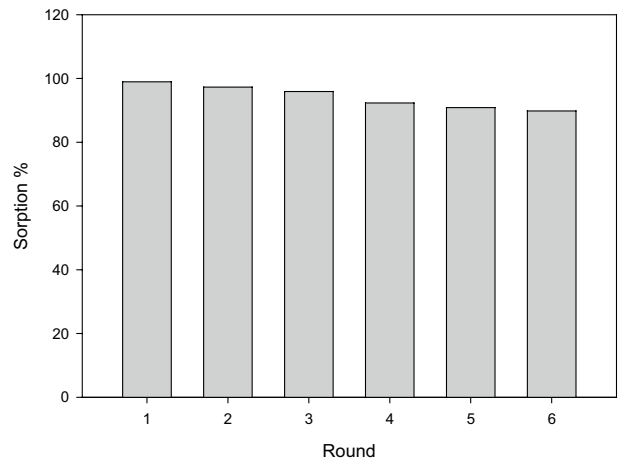


Fig. 13 Recycled efficiency of CTF nanoadsorbent in removal of U(VI)

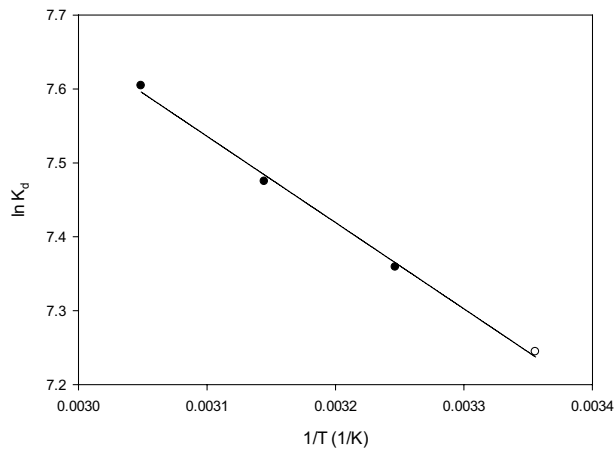


Fig. 12 Relationship curve between $\ln K_d$ and $1/T$

Table 5 Thermodynamic parameters for U(VI) adsorption onto CTF nanoadsorbent

| ΔH° (KJ mol ⁻¹) | ΔS° (J mol ⁻¹ K ⁻¹) | ΔG° (KJ mol ⁻¹) | | | |
|--|---|--|---------|---------|---------|
| | | 298 K | 308 K | 318 K | 328 K |
| 9.708 | 92.708 | -27.630 | -28.557 | -29.485 | -30.412 |

4 Conclusion

A synthesized magnetic CTF nanocomposite was successfully applied as a novel and effective sorbent for the removal of U(VI) from aqueous solutions either at low or high levels of uranium concentrations. The sorption ability of U(VI) on fabricated NPs was strongly dependent on

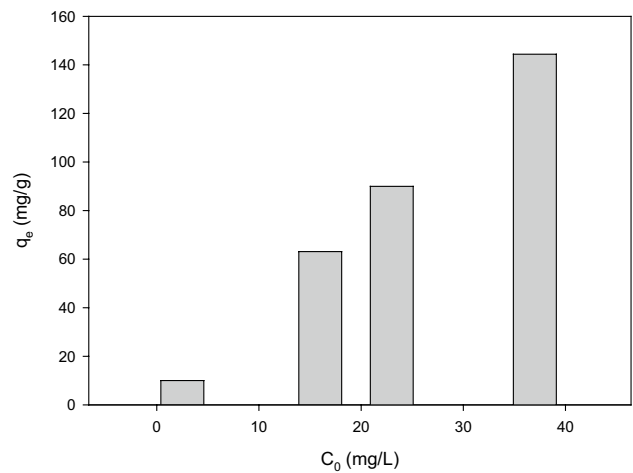


Fig. 14 CTF nanocomposite adsorption capacity towards U(VI) of waste solutions sample with different concentrations of U(VI) (2.5, 16, 23, 37 mg L⁻¹)

pH values. The sorption process was fast and 120 min was enough to achieve the sorption equilibration. The sorption isotherms of U(VI) on the prepared nanocomposite were described well by Freundlich and Halsey models and kinetically fitted with a pseudo-second-order model. The calculated thermodynamic parameters demonstrated that the endothermic heat of adsorption, and it was spontaneous. Easily desorbing of the adsorbed U(VI) from the synthesized nanocomposite several times makes the magnetic CTF nanocomposite act as a perfect adsorbent to remove uranium ions from solution at low and high concentrations.

Compliance with ethical standards

Conflict of interest The authors declare that they have no conflict of interest.

References

1. El-Ansary AL, Abd El-Wahab G, Bayoumi EE, Nouh ESA (2018) Purification of Abu-Zenima wet crude yellow cake using alkaline leaching of U (VI). *Egypt J Pet* 27:523–530
2. Nouh ESA, Amin MI, Gouda MM, Abd Almagid A (2015) Extraction of uranium (VI) from sulfate leach liquor after iron removal using manganese oxide coated zeolite. *J Environ Chem Eng* 3:523–528
3. Klimova S, Oernik M, Lacinova L, Filip J, Janick D, Zboril R (2011) Zero-valent iron nanoparticles in treatment of acid mine water from in situ uranium leaching. *Chemosphere* 82:1178–1184
4. International Atomic Energy Agency (2001) Handling and processing of radioactive waste from nuclear applications; TRS No. 402. IAEA, Vienna
5. Bhalara PD, Punetha D, Balasubramanian K (2014) A review of potential remediation techniques for uranium (VI) ion retrieval from contaminated aqueous environment. *J Environ Chem Eng* 2:1621–1634
6. Gu B, Liang L, Dickey MJ, Yin X, Dai S (1998) Reductive precipitation of uranium(VI) by zero-valent iron. *Environ Sci Technol* 32:3366–3373
7. Banning A, Benfer M (2017) Drinking water uranium and potential health effects in the German Federal State of Bavaria. *Int J Environ Res Public Health* 14:927
8. Collman GW, Loomis DP, Sandler DP (1991) Childhood cancer mortality and radon concentration in drinking water in North Carolina. *Br J Cancer* 63:626–629
9. Comarmond MJ, Payne TE, Collins RN, Palmer G, Lumpkin GR, Angove MJ (2012) Inhibition of uranium(VI) sorption on titanium dioxide by surface iron(III) species in ferric oxide/titanium dioxide systems. *Environ Sci Technol* 46:11128–11134
10. Amaral JCBS, Morais CA (2010) Thorium and uranium extraction from rare earth elements in monazite sulfuric acid liquor through solvent extraction. *Miner Eng* 23:498–503
11. Thakur P, Chakravorty P, Dash KC, Ramamohan TR, Reddy MLP (1998) Synergistic extraction of uranium (VI) by mixtures of β -diketones and structurally related crown ethers. *Radiochim Acta* 80:155–161
12. John AMS, Cattrall RW, Kolev SD (2010) Extraction of uranium(VI) from sulfate solutions using a polymer inclusion membrane containing di-(2-ethylhexyl) phosphoric acid. *J Membr Sci* 364:354–361
13. Ali AH, Nouh ESA (2018) Rhodamine-B modified silica for uranium(VI) extraction from aqueous waste samples. *Sep Sci Technol*. <https://doi.org/10.1080/01496395.2018.1512620>
14. Shaabana AF, Khalila AA, Lasheenb TA, Nouh ESA, Ammar H (2018) Polyamidoamine dendrimers modified silica gel for uranium(VI) removal from aqueous solution using batch and fixed-bed column methods. *Desalin Water Treat* 102:197–210
15. Nouh ESA, Roy M, Sarkar S (2012) Glucose stabilized magnetic palladium nanoparticles exhibiting enhanced magnetic properties under exposure to hydrogen. *Mater Express* 2:275–284
16. Veisheh O, Gunn JW, Zhang M (2010) Design and fabrication of magnetic nanoparticles for targeted drug delivery and imaging. *Adv Drug Deliv Rev* 62:284–304
17. Lu AH, Salabas EL, Schuth F (2007) Magnetic nanoparticles: synthesis, protection, functionalization, and application. *Angew Chem Int Ed* 46:1222–1244
18. Leal R, Yamaura M (2011) Equilibrium adsorption isotherm of U(VI) at pH 4 and pH 5 onto synthetic magnetite nanoparticles. *Int J Nucl Energy Sci Technol* 6:1–7
19. Wei J, Zhang X, Liu Q, Li Z, Liu L, Wang J (2014) Magnetic separation of uranium by CoFe_2O_4 hollow spheres. *Chem Eng J* 241:228–234
20. Tan L, Wang J, Liu Q, Sun Y, Jing X, Liu L, Liua J, Song D (2015) The synthesis of a manganese dioxide–iron oxide–graphene magnetic nanocomposite for enhanced uranium(VI) removal. *New J Chem* 39:868–876
21. Dutta P, Ray A, Sharma V, Millero J (2004) Adsorption of arsenate and arsenite on titanium dioxide suspensions. *J Colloid Interface Sci* 278:270–275
22. Engates KE, Shipley HJ (2011) Adsorption of Pb, Cd, Cu, Zn, and Ni to titanium dioxide nanoparticles: effect of particle size, solid concentration, and exhaustion. *Environ Sci Pollut Res* 18:386–395
23. Laurent S, Forge D, Port M, Roch A, Robic C, Elst LV, Muller RN (2008) Magnetic iron oxide nanoparticles: synthesis, stabilization, vectorization, physicochemical characterizations, and biological applications. *Chem Rev* 108:2064–2100
24. Spaldin N (2003) *Magnetic materials: fundamentals and device applications*. Cambridge University Press, Cambridge
25. Tan L, Liua Q, Jinga X, Liua J, Songa D, Hua S, Liub L, Wang J (2015) Removal of uranium(VI) ions from aqueous solution by magnetic cobalt ferrite/multiwalled carbon nanotubes composites. *Chem Eng J* 273:307–315
26. Zhang X, Wang J, Li R, Dai Q, Gao R, Liu Q, Zhang M (2013) Preparation of $\text{Fe}_3\text{O}_4@\text{C}$ layered double hydroxide composite for magnetic separation of uranium. *Ind Eng Chem Res* 52:10152–10159
27. Fan FL, Qin Z, Bai J, Rong WD, Fan FY, Tian W, Wu XL, Wang Y, Zhao L (2012) Rapid removal of uranium from aqueous solutions using magnetic $\text{Fe}_3\text{O}_4@\text{SiO}_2$ composite particles. *J Environ Radioact* 106:40–46
28. Zong P, Gou J (2014) Rapid and economical synthesis of magnetic multiwalled carbon nanotube/iron oxide composite and its application in preconcentration of U(VI). *J Mol Liq* 195:92–98
29. Tan L, Zhang X, Liu Q, Jing X, Liu J, Song D, Hu S, Liu L, Wang J (2015) Synthesis of $\text{Fe}_3\text{O}_4@\text{TiO}_2$ core-shell magnetic composites for highly efficient sorption of uranium(VI). *Colloids Surf A Physicochem Eng Asp* 469:279–286
30. Mirzabe G, Keshtkar A (2015) Selective sorption of U(VI) from aqueous solutions using a novel aminated $\text{Fe}_3\text{O}_4@\text{SiO}_2/\text{PVA}$ nanofiber adsorbent prepared by electrospinning method. *J Radioanal Nucl Chem* 303:561–576
31. Wazne M, Korfiatis GP, Meng X (2003) Carbonate effects on hexavalent uranium adsorption by iron oxyhydroxide. *Environ Sci Technol* 37:3619–3624
32. El-sherif RM, Lasheen TA, Jebri EA (2017) Fabrication and characterization of $\text{CeO}_2\text{-TiO}_2\text{-Fe}_2\text{O}_3$ magnetic nanoparticles for rapid removal of uranium ions from industrial waste solutions. *J Mol Liq* 241:260–269
33. Marczenko Z (1986) *Separation and spectrophotometric determination of elements*. Ellis Harwood, Chichester
34. Maity D, Chandrasekharan P, Si-Shen F, Xue JM, Ding J (2010) Polyol-based synthesis of hydrophilic magnetite nanoparticles. *J Appl Phys* 107(09B310):1–3
35. Dyer JR (1965) *Application of organic compound*, 6th edn. Prentice-Hall, Englewood Cliffs
36. Kumar S, Kumar P, Singh V, Mandal UK, Konala RK (2015) Synthesis, characterization and magnetic properties of monodisperse Ni, Zn-ferrite nanocrystals. *J Magn Magn Mater* 379:50–57

37. Manos MJ, Kanatzidis MG (2012) Layered metal sulfides capture uranium from seawater. *J Am Chem Soc* 134:16441–16446
38. Zhu L, Yuan L-Y, Xia L-S, Wang L (2016) Incorporation of magnetism into the dihydroimidazole functionalized mesoporous silica for convenient U(VI) capture. *J Radioanal Nucl Chem* 308:447–458
39. Wang F, Li H, Liu Q, Li Z, Li R, Zhang H, Liu L, Emelchenko GA, Wang J (2016) A graphene oxide/amidoxime hydrogel for enhanced uranium capture. *Sci Rep* 6:1–8
40. Khanna L, Verma NK (2014) Synthesis, characterization and biocompatibility of potassium ferrite nanoparticles. *J Mater Sci Technol* 30(1):30–36
41. Laokul P, Amornkitbarmung V, Seraphin S, Maensiri S (2011) Characterization and magnetic properties of nanocrystalline CuFe_2O_4 , NiFe_2O_4 , ZnFe_2O_4 powders prepared by the Aloe vera extract solution. *Curr Appl Phys* 11:101–108
42. Sheng GD, Yang ST, Sheng J, Zhao DD, Wang XK (2011) Influence of solution chemistry on the removal of Ni(II) from aqueous solution to titanate nanotubes. *Chem Eng J* 168:178–182
43. Moulin C, Laszak I, Moulin V, Tondre C (1998) Time-resolved laser-induced fluorescence as a unique tool for low-level uranium speciation. *Appl Spectrosc* 52:528–535
44. Guerra DL, Viana RR, Airoidi CJ (2009) Adsorption of thorium cation on modified clays MTTZ derivative. *J Hazard Mater* 168:1504–1511
45. Abbasi WA, Streat M (1994) Adsorption of uranium from aqueous solutions using activated carbon. *Sep Sci Technol* 27:1217–1230
46. Yuan L-Y, Liu Y-L, Shi W-Q, Lv Y-L, Lan J-H, Zhao Y-L, Chai Z-F (2011) High performance of phosphonate-functionalized mesoporous silica for U(VI) sorption from aqueous solution. *Dalton Trans* 40:7446–7453
47. Bonato M, Ragnarsdottir KV, Allen GC (2012) Removal of uranium(VI), lead(II) at the surface of TiO_2 nanotubes studied by X-ray photoelectron spectroscopy. *Water Air Soil Pollut* 223:3845–3857
48. Watanabe T, Ikeda Y (2013) A study on identification of uranyl complexes in aqueous solutions containing carbonate ion and hydrogen peroxide. *Energy Proc* 39:81–95
49. Nilchi A, Dehaghan TS, Garmarodi SR (2013) Kinetics, isotherm and thermodynamics for uranium and thorium ions adsorption from aqueous solutions by crystalline tin oxide nanoparticles. *Desalination* 321:67–71
50. Anirudhan TS, Sreekumari SS (2010) Synthesis and characterization of a functionalized graft copolymer of densified cellulose for the extraction of uranium(VI) from aqueous solutions. *Colloids Surf A Physicochem Eng Asp* 361:180–186
51. Kamari A, Ngah WSW, Chong MY, Cheah ML (2009) Sorption of acid dyes onto GLA and H_2SO_4 cross-linked chitosan beads. *Desalination* 249:1180–1189
52. Sabarudin A, Oshima M, Takayanagi T, Hakim L, Oshita K, Gao YH, Motomizu Sh (2007) Functionalization of chitosan with 3,4-dihydroxybenzoic acid for the adsorption/collection of uranium in water samples and its determination by inductively coupled plasma-mass spectrometry. *Anal Chim Acta* 581:214–220
53. Sheng G, Li Y, Dong H, Shao D (2012) Environmental condition effects on radionuclide $^{64}\text{Cu}(\text{II})$ sequestration to a novel composite: polyaniline grafted multiwalled carbon nanotubes. *J Radioanal Nucl Chem* 293:797–806
54. Yang S, Guo Z, Sheng G, Wang X (2012) Investigation of the sequestration mechanisms of Cd(II) and 1-naphthol on discharged multi-walled carbon nanotubes in aqueous environment. *Sci Total Environ* 420:214–221
55. Sun Y, Yang Sh, Sheng G, Guo Z, Wang X (2012) The removal of U(VI) from aqueous solution by oxidized multiwalled carbon nanotubes. *J Environ Radioact* 105:40–47
56. Sheng G, Dong H, Shen R, Li Y (2013) Microscopic insights into the temperature-dependent adsorption of Eu(III) onto titanate nanotubes studied by FTIR, XPS, XAFS and batch technique. *Chem Eng J* 217:486–494
57. Bhatnagar A, Jain AK (2005) A comparative adsorption study with different industrial wastes as adsorbents for the removal of cationic dyes from water. *J Colloid Interface Sci* 28:49–55
58. Hu X, Wang J, Liu Y, Li X, Zeng G, Bao Z, Zeng X, Chen A, Long F (2011) Adsorption of chromium (VI) by ethylenediamine-modified cross-linked magnetic chitosan resin: isotherms, kinetics and thermodynamics. *J Hazard Mater* 185:306–314
59. Hameed BH (2009) Removal of cationic dye from aqueous solution using jackfruit peel as non-conventional low-cost adsorbent. *J Hazard Mater* 162:344–350
60. Kilincarslan A, Akyil S (2005) Uranium adsorption characteristic and thermodynamic behavior of clinoptilolite zeolite. *J Radioanal Nucl Chem* 264:541–548
61. Zong PF, Wang SF, Zhao YL, Wang H, Pan H, He CH (2013) Synthesis and application of magnetic graphene/iron oxides composite for the removal of U(VI) from aqueous solutions. *Chem Eng J* 220:45–52
62. Zhao YG, Li JX, Zhao LP, Zhang SW, Huang YS, Wu XL, Wang XK (2014) Synthesis of amidoxime-functionalized $\text{Fe}_3\text{O}_4@/\text{SiO}_2$ core-shell magnetic microspheres for highly efficient sorption of U(VI). *Chem Eng J* 235:275–283
63. Banerjee C, Dudwadkar N, Tripathi SC, Gandhi PM, Grover V, Kaushik CP, Tyagi AK (2014) Nano-cerium vanadate: a novel inorganic ion exchanger for removal of americium and uranium from simulated aqueous nuclear waste. *J Hazard Mater* 280:63–70